Design and Simulation of an Electrostatic Energy Harvester for Biomedical Implants

Francisco Ambia, Jhordan Chavez, Mickael Lallart, Xavier Leroux, Elie Lefeuvre

Design and Simulation of an Electrostatic Energy Harvester for Biomedical Implants

Francisco Ambia
Centre de Nanosciences et de Nanotechnologies (C2N)
Université Paris Saclay, 3 rue Joliot Curie
Gif-sur-Yvette, France
jose-francisco.ambia-campos@universite-paris-saclay.fr

Jhordan Chavez
Centre de Nanosciences et de Nanotechnologies (C2N)
Université Paris Saclay, 3 rue Joliot Curie
Gif-sur-Yvette, France
jhordan.chavez@universite-paris-saclay.fr

Mickaël Lallart
Laboratoire LGEF
INSA de Lyon, 8 Rue de la physique
Villeurbanne, France
mickael.lallart@insa-lyon.fr

Xavier Leroux
Centre de Nanosciences et de Nanotechnologies (C2N)
Université Paris Saclay, 3 rue Joliot Curie
Gif-sur-Yvette, France
xavier.leroux@universite-paris-saclay.fr

Elie Lefeuvre
Centre de Nanosciences et de Nanotechnologies (C2N)
Université Paris Saclay, 3 rue Joliot Curie
Gif-sur-Yvette, France
elie.lefeuvre@universite-paris-saclay.fr

2021 Symposium on Design, Test, Integration & Packaging of MEMS and MOEMS (DTIP) | 978-1-6654-0230-9/21/$31.00 ©2021 IEEE | DOI: 10.1109/DTIP54218.2021.9568675

***Abstract*— This paper presents the design of an electrostatic MEMS energy harvester for medical implant application. It examines solutions for constraining the motion of the mobile part in one direction and proposes an innovative spring architecture. Indeed, constraining the mobile part motion is essential to avoid undesired contact between comb electrodes. It is particularly important in environments in which mechanical vibrations result from complex combination of rotations and translations. The objective of the considered device is to power the next generation of leadless pacemakers using mechanical energy generated by heartbeat motion. Such solution would dramatically increase the lifetime of implants and would be very beneficial for the patients by reducing the number of replacement surgical operations. Numerical simulations based on analytical modelling and acceleration signal mimicking heartbeat motion enabled to analyze the system response in various condition, showing the interest and benefits of the proposed approach.**

Keywords—Energy harvesting, MEMS, electrostatic transducer, heartbeat, low frequency, medical implant.

I. INTRODUCTION

Vehicles [1], buildings [2], wearables, biomedical implants [3], all rely on sensors and circuits that need electrical energy to work. Usually, such devices are provided with energy and information through cables, but it may not always be possible to connect them physically due to their location. Wireless connection is an interesting alternative, as it increases flexibility and reliability for the vast majority applications, enabling the devices to be located in harsh environments and places difficult to reach [3]. While wireless devices present numerous advantages, the way their energy autonomy can be insured in the long term remains a challenge of active research.

Energy harvesting (EH) solutions have gained an important interest over the last decade due to their ability to extract energy from the environment and provide it to low power electronic devices. While most of the applications of EH are related to power wireless sensor networks (IoT) [4], there are other interesting applications such as powering biomedical implants from human motion [5]. As for IoT, harvested energy may be used for data acquisition and transmission for biomedical implants, but also can be used to assist or replace a bodily function, examples of this are insulin pumps or pacemakers [6] [7].

Although at first glance it may seem counterintuitive to harvest energy from a defective heart, such approach would decrease the number of surgical interventions to replace a depleted battery, hence reducing the risk of infection and complications during treatment. In [8] it is shown that cardiac implants have an average lifetime of 58 months, besides 8% of the implants present a premature battery depletion by three years. We see an imperative need of extending the lifetime of cardiac implants. Kinetic EH is a viable solution to this problem making the treatment less risky and comfortable for the patient. The new generation of leadless pacemakers are meant to be implanted inside the heart right atrium with a probe [5], this is very comfortable for the patient but it imposes a restriction on available space for the design. For this application, our device should enter in a cylindrical cavity of 5mm diameter and 2cm long.

Among different available transduction mechanisms to transform mechanical energy into electricity, the most common ones are based on piezoelectricity [5], electromagnetism [9] and electrostatic transduction [10]. Each one has its own advantages and disadvantages with respect to the others, considering aspects such as power density, fabrication cost, miniaturization and easiness of integration. Electrostatic MEMS solution is particularly interesting due to its easiness of integration with CMOS platforms and the fact that MEMS fabrication technologies can be relatively easily upscaled to mass production.

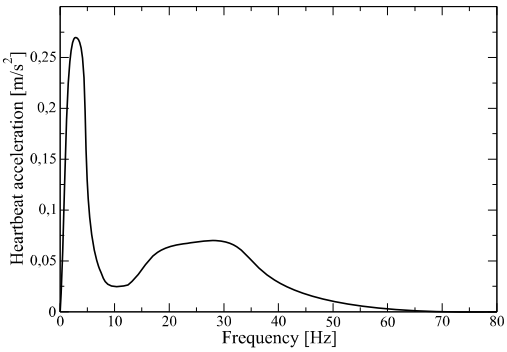

Fig.1. Heartbeat spectrum (qualitative approximation, acctual acceleration may vary largly from this figure) from [5]

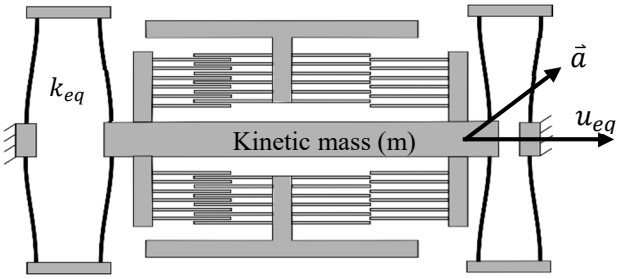

Fig.2. Electrostatic transducer on non parell driving acceleration

II. Driving Acceleration

The first aspect to consider for energy harvesting is the acceleration's power spectrum. The acceleration produced by the heartbeat has typically low frequencies and spread over a large bandwidth. Fig.1 shows a qualitative illustration of the acceleration spectrum of the heartbeat [5]. Most of the useful spectrum is below 80Hz. Ideally, we would like to take all these frequencies but as we will see later, we need to make design compromises.

The second aspect to consider is the orientation of the device with respect to the gravity field. We would like our device to work in a wide range of orientations, no matter if the patient with the implant is standing or laying on bed, the harvester should work in any case. This brings gravity into play, whose effect on the EH device will be detailed in the next section.

Finally, the heart-beat acceleration in not unidirectional. It results from a complex combination of rotations and translations. Despite this, the structure of the MEMS must be able to constrain the movement of its mobile part in one direction only (Fig.2) to avoid unwanted contact between the transducer fixed and mobile electrodes.

III. Spring Design

The aim of the spring is to enable engagement and disengagement of the capacitor combs driven by an inertial force and at the same prevent them to come into contact. To prevent contact, the spring design should allow free movement along one axis only, corresponding to the direction where the combs engage and disengage.

The vast majority of MEMS devices rely on compliant elements such as beams [11] or membranes [12]. We consider here several configurations of beams with rectangular sections and we assess the ability of a given configuration to constrain motion.

The following notation is used for displacements (Fig.2): u_{eq} represents the displacement in the direction of motion where the combs engage, u_{per} is an in-plane perpendicular displacement where combs may come into contact and u_{out} represents an out-of-plane displacement.

In terms of displacements, having a good movement constriction means $u_{eq} \gg u_{per}, u_{out}$. Considering that the device can be in any orientation with respect to acceleration, the magnitude of the inertial force F exerted on the moving part can be the same for all directions, meaning that spring constants $k_{per}\ and\ k_{out}$ must be much larger than k_{eq} ($k_i = F/u_i$).

As mentioned before, all the compliant elements of the system are beams of rectangular section. These parts are the red elements in Fig.3, while rigid and free to move elements are in blue. All the red elements are considered as doubly clamped beams with a punctual load at the end conserving their length constant when deformed, meaning that one end of the beam moves perpendicular to the deformation to maintain a constant length. Allowing the beams to remain at constant length avoids non-linear terms related to stretching. Equation (1) is the spring constant of a single beam with a force in u_{eq} direction, where E is the Young's Modulus, L is the beams length, and H is the beams width and W is the thickness of the device. This expression was derived with the energy method described in [13].

$$k_{eq} = \frac{\pi^4}{96} EW \left(\frac{H}{L}\right)^3 \tag{1}$$

The perpendicular displacement of the beam can be calculated from the beams shape considering the case of small slopes, the perpendicular displacement reads as (2).

$$u_{per} = -\frac{\left(\pi u_{eq}\right)^2}{16L} \tag{2}$$

The first considered geometry is the folded spring (FS, Fig.3). This geometry is frequently found in MEMS devices. It yields a linear force-displacement relation and if the force is parallel to u_{eq}. When a force u_{per} is applied, a relatively weak opposing force is obtained ($k_{per} \sim k_{eq}$). Such weak opposing force comes from the fact that the beam supports are free to rotate, making easy to move the shuttle in u_{per} direction. Therefore, using the FS geometry alone, the capacitor combs of the electrostatic transducer risk to come in contact when the inertial force is in u_{per} direction.

The second considered geometry is the Opposing Beams (OB, Fig.3). This geometry is very beneficial for constraining motion in terms of spring constants. When we apply a force in u_{per} direction the beams will load axially the beams. Assuming that the force is not large enough to buckle the beams, the spring constants grows as $k_{per} \sim k_{eq}(L/H)^2$. As mentioned before, we consider that all beams keep their length constant when deformed, making the beams moving end follow the trajectory described by (2). While OB geometry provides a large restoring force in u_{per} direction, the u_{per} displacement induces a non-negligible rotation in

the mobile part that may cause contact between the mobile and fixed combs.

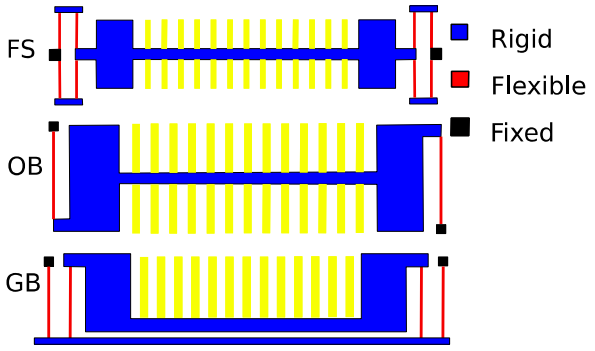

Fig.3. Studied spring geometries. Red elements are compliant and free to move, blue are rigid and free to move while black are completely fixed. Yellow regions represent the space avalaible for the transducer combs.

TABLE 1. COMPARSION BETWEEN FEM AND THEORETICAL SPRING CONSTANTS FOR GUIDIING BEAMS GEOMETRY

	Theoretical [N/m]	*FEM[N/m]*	*Difference*
k_{eq}	10.0608	0.9823*k_{eq}	1.77%
k_{out}	50* k_{eq}	58.6235* k_{eq}	17.24%
k_{per}	1935.2252* k_{eq}	2121.9574* k_{eq}	9.65%

One can understand this rotation in the following way: when the shuttle moves to the right, to keep constant length, the end of the left beam would need to move up while the right beam end would move down, resulting in a clockwise rotation of the shuttle. This rotation motion revealed to be too large in magnitude regarding the constraints of our application.

To overcome to the limitations and drawbacks of the two previous designs, we proposed the guided beam geometry (GB, Fig.3). This geometry can be considered as two nested parallel guiding compliant mechanisms presented in [14] or half the one in [15]. Compared to former geometries, this new one has a smaller footprint and leaves more space for the combs. Like the FS geometry, GB neutralizes the perpendicular displacement of (2) by placing two opposing beams in each side of the shuttle. The free supports get closer to the shuttle and the mobile part remains always in the same orientation axis.

The overall spring constant of GB geometry is the same as for a single beam in (1). The GB geometry is very similar to FS one. The difference between the two is that in the GB case there is guiding beam that connects the two moving beam supports which are independent in the FS case. This supplementary guiding beam removes the degree of freedom that causes a weak restoring force in u_{per} for the FS case. Adding the guiding beam transforms the beam support rotation in the FS case into a bending moment to the guiding beam. The spring constant in this direction is obtained by considering the guiding beam as doubly supported beam with two symmetric punctual loads separated by a distance a from the support. Equation (3) describes the springs constant in u_{per} direction, L_{GB} and H_{GB} are the guiding beam length and width respectively while H is the width of the doubly clamped beam.

$$k_{per} = \frac{48}{\pi^4(3a^2L_{GB} - 4a^3)}\left(\frac{L_{GB}H_{GB}}{H}\right)^3 k_{eq} \tag{3}$$

The spring constant in u_{out} direction can be calculated changing in (1) u_{eq} for u_{out}, H for W and vice-versa W for H. We see that deforming the beam in u_{eq} and u_{out} directions are equivalent cases for different cross-sections. One can deduct from (1) that the spring constant grows as: $k_{out} \sim (W/H)^2 k_{eq}$. Despite the GB geometry does not provide a restoring force as strong as the OP one in u_{per} direction, it maintains the mobile part well aligned and ensures the best mobile part movement guidance for the considered application.

IV. DESIGN PARAMETERS

The device should enter in a cylindrical cavity with a diameter of 5 mm and length of 2 cm. The available space is the first design constraint. The second one is the heartbeat spectrum, and the third aspect to consider is the shuttle displacement range related to the yield stress of the structure and the mechanical energy that can come into the system, as described in [16] and [17].

Considering the GB spring geometry, with $L = 3010\mu m$, $H = 20\mu m$, $W = 200\mu m$, $L_{GB} = 15mm$ and $H_{GB} = 200\mu m$ the spring constants in each direction are given in TABLE *1*. This table compares analytical predictions based on the study described in the previous section and FEM simulations. One can see analytical predictions for spring constant match well with the FEM simulations. A larger difference for k_{out} is due to the asymmetry of the GB geometry, which makes the beams clamped between the guiding beam and the shuttle to behave closer to a cantilever rather than a doubly clamped beam in the out-of-plane direction.

The dimensions were chosen so that the maximum stress is less than $700\,MPa$ for a total shuttle traveling range of $600\,\mu m$, meaning $u_{eq} = \pm 300\,\mu m$. The maximum stress found in the joints of the beams was estimated as $\sigma_{max} = 0.25EHu_{eq,max}(\pi/L)^2$. for $u_{eq,max} = 300\,\mu m$, the maximum stress was $\sigma_{max} = 278$ MPa, which is far below the considered $700\,MPa$ limit. This analytical prediction was confirmed by FEM simulation.

Let us ignore for a moment the electrostatic forces between the combs and consider the system as a damped harmonic oscillator in each direction, a single mass coupled by three springs. In the equation (4) that models the three springs coupled to the same mass with same quality factor Q, we consider the driving acceleration as a sinusoid to get the frequency response of the oscillator. In this equation, $i = \{eq, per, out\}$ and $\vec{g} \cdot \hat{u}_i$ is the projection of gravity in the direction u_i and $\omega_{n,i} = k_i/m$.

The desired inertial mass will be obtained in practice by adding a supplementary tungsten mass on top of the silicon shuttle.

$$\ddot{u}_i + \frac{\omega_{n,i}}{Q}\dot{u}_i + \omega_{n,i}^2 u_i = a_{ext}\sin(\omega t) + \vec{g} \cdot \hat{u}_i \tag{4}$$

$$u_{i,pp} = \frac{a_{ext}}{\sqrt{\left(\frac{\omega\omega_{n,i}}{Q}\right)^2 + \left(\omega_{n,i}^2 - \omega^2\right)^2}} \quad (5)$$

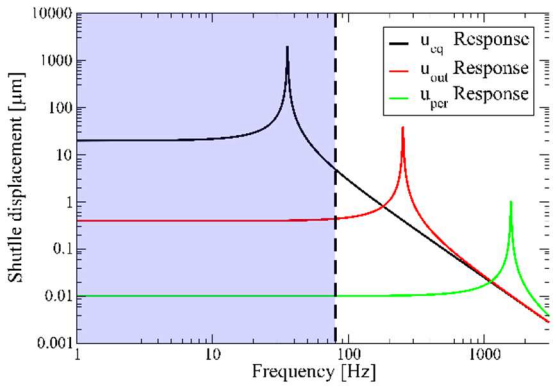

Fig.4 Displacement vs. frequency displacement in the three directions u_{eq}, u_{per} and u_{out}. The region in blue corresponds to the domain of frequencies where lays the heartbeat acceleration spectrum.

The offset Δu_i that gravity imposes on the shuttle is given by (6). This offset was calculated as the average in time $\Delta u_i = \langle u_i \rangle_t$ of the stationary solution u_i of (4).

$$\Delta u_i = \frac{\vec{g} \cdot \hat{u}_i}{\omega_{n,i}^2} \quad (6)$$

In a similar way, the movement amplitude can be calculated by taking the RMS value ${u_{i,rms}}^2 = \langle (u_i - \Delta u_i)^2 \rangle_t$ and transforming it into an peak to peak value for a sinusoidal ${u_{i,pp}}^2 = 2{u_{i,rms}}^2$, leading to equation (5).

Now the MEMS mechanical model has been defined, one can define the remaining system parameter m and Q. The value of the quality factor Q results from different mechanical loss mechanisms. Based on experimental results of similar MEMS devices [18], we assume the quality factor to be around 100 in all directions.

We chose to place a tungsten supplementary mass of $0.2\ mg$ on top of the shuttle. According to (6), in the worst case we get the offsets $\Delta u_{eq} = 196\ \mu m$, $\Delta u_{out} = 3.9\ \mu m$ and $\Delta u_{per} = 0.1\ \mu m$. These worst-case offsets are calculated assuming that gravity is perfectly aligned with the considered direction, yielding the maximum offset for each case.

We see that the offset Δu_{eq} would take two thirds of the total displacement range of the device $u_{eq,max}$. This will reduce the amplitude of the capacitance variation, reducing at the same time the recuperated energy in each cycle. The effect of gravity and the offset on the recuperated energy will be analyzed in detail in the simulation section. The worst-case offset Δu_{out} will reduce the surface of the capacitor to about 2% of its nominal value. Finally, the offset Δu_{per} will be taken ito account to study its effect on the electrostatic force acting between the fixed and moving combs.

Fig.4 shows the peak-to-peak displacement calculated from (5) of the shuttle in the three dimensions as a function of frequency considering a driving acceleration a_{ext} of $1\ m/s^2$. The area in blue is the frequency region where lays the heartbeat acceleration spectrum. One can see that the response for u_{per} and u_{out} in the blue region is negligible compared to u_{eq}, confirming the suitability of the spring geometry to constrain the motion of the MEMS shuttle in the desired direction.

V. Electromechanical Model

In this section we consider a linear damped harmonic oscillator driven by a heartbeat acceleration, adding stoppers that keep the shuttle in a delimited region and an electrostatic transducer driven by an ideal charge pump circuit, similarly to the Roundy charge pump [19]. First, we perform a set of simulations with an ideal charge pump as interface circuit to determine the most adequate interface circuit for the device. The choice of the circuit will depend on the ratio $\gamma = V_{max}/V_{min}$ that yields the maximum power output.

A. Mechanical Domain

As shown in the previous section, the only displacement sensible to the heartbeat acceleration is u_{eq}. Therefore, a single degree of freedom harmonic oscillator was considered here. For simplicity in notation in this section, u_{eq} will be simply u and $\omega_{n,eq} = \omega_n$.

In (4) we excited the system with a sinusoidal acceleration, in (7) we drive the system with a time series of a heartbeat acceleration signal. Two nonlinear forces F_{stop} and F_{elec} that represent the stoppers and force exerted by the combs respectively were added in the equation.

$$\ddot{u} + \frac{\omega_n}{Q}\dot{u} + \omega_n^2 u = a_{ext} + g\cos(\theta) + \frac{F_{elec}}{m} + \frac{F_{stop}}{m} \quad (7)$$

Variable $u(t)$ is the kinetic mass position, $\omega_n^2 = k_{eq}/m$ is the natural frequency, Q is the quality factor, g is gravity acceleration, a_{ext} is the driving external acceleration, θ is the angle between gravity and shuttle movement directions, F_{elec} is the electrostatic force that allows energy conversion and finally F_{stop} that maintain the mass between $-u_{max}$ and u_{max}.

We consider stoppers as flexible-dissipating walls with high spring constants $k_{stop} \gg k_{eq}$ and μ_{stop} damping coefficients that dissipate energy at each time the moving part hits the limiting wall at $\pm u_{max}$, we may express the stopper force as:

$$F_{stop} = \begin{cases} -k_{stop}(u + u_{max}) - \mu_{stop}\dot{u}, & u < -u_{max} \\ 0, & -u_{max} \le u \le u_{max} \\ -k_{stop}(u - u_{max}) - \mu_{stop}\dot{u}, & u > u_{max} \end{cases} \quad (8)$$

From (8) we see the importance of knowing the offset Δu_{eq}, we need to choose a right pulsation ω_n^2 in such a way that $u_{eq,max} > \Delta u_{eq}$, otherwise the mass would always stay stuck to the stopper and no energy conversion effect will be obtained.

B. Electrostatic domain

The MEMS variable capacitor value that depends on the shuttle position u. Amongst several possible geometries for the variable capacitor, the area overlap geometry schematically depicted in Fig.5 was chosen to avoid squeeze film damping effects [18].

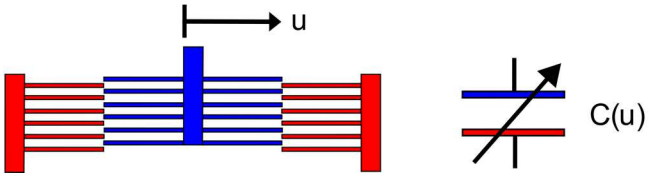

Fig.5. Area overlap variable capacitor. In red we see fix electrodes and blue the free electrode attached to the shuttle.

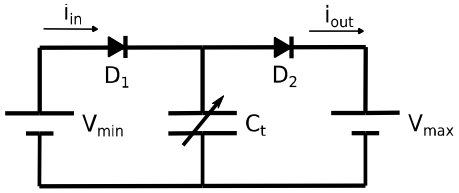

Fig.6. Ideal charge pump circuit.

The dependence of capacitance in position can be approximated as:

$$C(u_{eq}) = N\frac{\varepsilon_0 W}{gap}\begin{cases} -u_{eq}, & u_{eq} < -\alpha \\ \alpha, & -\alpha \le u_{eq} \le \alpha \\ u_{eq}, & u_{eq} > \alpha \end{cases} \quad (9)$$

In this expression, $N\ is$ the number of comb fingers, ε_0 is vacuum permittivity, W is device thickness and α a positive value that defines the minimal capacitance C_{min}.

We check the stability of the comb fingers and see up to which value of voltage we can go before pull-in. A figure of merit (10) defined in [5] will serve us to determine the range of values for which our comb fingers are stable.

$$FoM = \frac{EH_F^3 gap^3}{3\varepsilon_0 L_F^3 V_c^3} \quad (10)$$

Where E is Youngs Modulus, H_F is the fingers width, fingers length L_F and V_c the voltage between the electrodes. The force exerted between the moving and fixed combs is calculated as:

$$F_{elec} = \frac{1}{2}\frac{dC}{du}V_c^2 \quad (11)$$

This force and the displacement define the energy conversion mechanism. The electrical power is obtained by multiplying the voltage across the capacitor V_c and the current flowing through the capacitor. *T*his should be equal to the mechanical power extracted through the effect of the electrostatic force: $\langle V_{max} i_{out} + V_{min} i_{in}\rangle_t = \langle \mathrm{F_{elec}}\dot{x}\rangle_t$ (Fig.6).

To determine the working voltages in the transducer that yield the maximum harvested power, the electrostatic transducer was connected to an ideal charge pump interface circuit (Fig.6). the ratio $\gamma = V_{max}/V_{min}$ was varied to find the number of cells of the actual interface circuit [20] needed to maximise the output power.

VI. Simulations

We solved numerically (7) given that there is no analytical solution. The simulations were performed plugging into a_{ext} a heartbeat acceleration recording, the electrostatic force (11) was driven by the circuit of Fig.6. The simulations were performed using Ngspice environment by taking an electrical analogue circuit of the electromechanical system described by (7).

All presented simulations were performed considering the GB geometry with $m = 0.2g$, $k_{eq} = 10.06N/m$, and $Q = 100$. The variable capacitance consists on a total of 1452 capacitor comb fingers. Note that half of the capacitor are engaged to one side and the half to the other side, resulting on N = 726 capacitor comb fingers for each side. When engaged, the combs are separated by a $4\mu m\ gap$. The wafer thickness is $W = 200\,\mu m$, considering a parasitic capacitance of $C_{min} = 20\,pF$ which translates to $\alpha =$ 62.23 µm.

The maximum capacitance $C_{max} = 96.42\,pF$ was obtained at maximum displacement $u_{eq,max}$ and (9). The dimentions of the combs were chosen in a way so that we maximise the capacitance value for the pull-in and space constraints.

For the stoppers we assumed that their quality factor was two orders of magnitude bigger that the shuttle $Q_{stopper} = 100Q$, while the restoring force we assumed that it was three orders of magnitude $k_{stopper} = 1000k_{eq}$. This way we consider $Q_{stopper}$ so that each time the shuttle touches the stopper, it dissipates energy, but less than the loss due to friction between the air and the combs. At the same time, we chose $k_{stopper}$ in such a way so that the bouncing is almost immediate compared to the dynamics of the shuttle but not too big to make the simulation unstable.

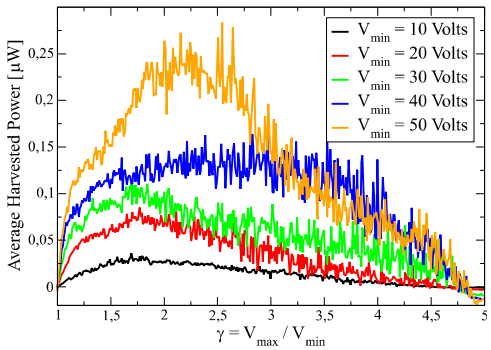

Fig.7. Exploration of the (V_{max}, V_{min}) dependance of the harvested power.

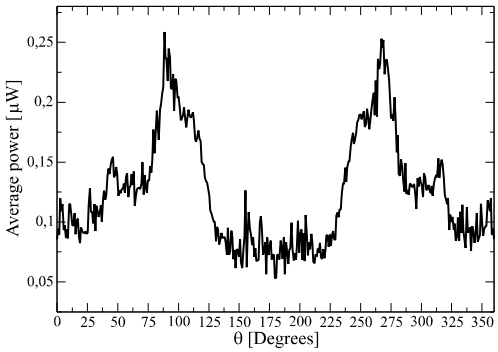

Fig.8. Harvested power as a function of orientation of the device with respect to gravity. Zero degrees corresponds to the device orineted in such a way that gravity is aligned with the shuttle movement direction.

The first set of simulations in Fig.7 were done without the influence of gravity. The aim of the first set of simulations was to find the optimal value of $\gamma = V_{max}/V_{min}$, the ratio that yields the maximum power. In [21], the optimal value for $\gamma = 0.5(1 + C_{max}/C_{min})$ was found, this expression is valid for systems that pass though their maximal and minimal

capacitances at each QV cycle. For a heartbeat driving acceleration we cannot suppose this, the heartbeat has a stochastic behavior both in time and amplitude. This makes an irregular set of QV cycles, the harvested power shown in Fig.7 and Fig.8 were calculated averaging all QV cycles letting the simulation run and calculate the average harvested power at the end of each simulation.

Five subsets of simulations were performed taking as a reference $V_{min} = \{10V, 20V, 30V, 40V, 50V\}$. Values close to $\gamma = 1$ have zero harvested power because the QV cycle has side $(V_{max} - V_{min})$ zero and the harvested energy of each cycle is $(C_{max}V_{min} - C_{min}V_{max})(V_{max} - V_{min})$. Doing simulations for different values of γ, it was found that in average the optimal value of γ is around two, which means that the best interface circuit for this particular device should be a one cell circuit from [20]. Note that this varies from the prediction of [21] where the optimal ratio should be $\gamma = 3$ under the assumption the capacitance passes through its extremum at each cycle.

Once the best performing circuit configuration was found, we studied the impact on harvested power of the device orientation with respect to gravity. In Fig.8 the dependance of harvested power on different device orientations is depicted, these simulations were done considering the best voltage configurations $\gamma = 2$. A maximum of $0.25\mu W$ for $\theta = 90°$ and $\theta = 270°$ were found, this is the case where the shuttle movement is perpendicular to gravity. When gravity pulls directly on the shuttle $\theta = 0°$ and $\theta = 180°$ the harvester power drops to $0.1\mu W$ due to the offset (6) induced by gravity, this forbids the combs to engage and disengage completely at each cycle.

VII. Conclusions

We explored different spring designs for guiding the shuttle and prevent the combs to come into contact. This study led us to propose the novel GB spring design, which enables to place the resonant frequencies in u_{per} and u_{out} directions far from the heartbeat spectrum, and at the same time to favor u_{eq} movement in this range of frequencies. This study proved that the GB geometry will forbid contact between the moving and fixed combs under heartbeat acceleration in any orientation of the MEMS.

We proposed and solved numerically the complete electromechanical model of the system. This theoretical study enabled to determine the harvested power. It also enabled to determine the effect of gravity on the harvested power.

The harvested power obtained by simulation is about one order of magnitude lower than the required power for the pacemaker application. Future studies will aim at investigation solutions enabling to increase the harvested power by increasing the inertial mass and the operating voltages.

Ongoing works on microfabrication will aim to compare the theoretical predictions with measurements performed on real MEMS devices to assess and refine the model.

Acknowledgment

Dimitri Galayko for his insightful discussions on the simulation of MEMS systems with spice.

References

[1] X. D. Xie and Q. Wang, "Energy harvesting from a vehicle suspension system," *Energy*, vol. 86, pp. 385–392, 2015.

[2] X. D. Xie, N. Wu, K. V. Yuen, and Q. Wang, "Energy harvesting from high-rise buildings by a piezoelectric coupled cantilever with a proof mass," *International Journal of Engineering Science*, vol. 72, pp. 98–106, 2013.

[3] M. A. Hannan, S. Mutashar, S. A. Samad, and A. Hussain, "Energy harvesting for the implantable biomedical devices: issues and challenges," *Biomedical engineering online*, vol. 13, no. 1, pp. 1–23, 2014.

[4] D. Galayko, A. Karami, P. Basset, and E. Blokhina, "Kinetic energy harvesting for the IoT: Perspectives and challenges for the next decade," in *2018 25th IEEE International Conference on Electronics, Circuits and Systems (ICECS)*, 2018, pp. 593–596.

[5] M. Deterre, "Toward an energy harvester for leadless pacemakers," PhD Thesis, Paris 11, 2013.

[6] J. Paulo and P. Gaspar, "Review and Future Trend of Energy Harvesting Methods for Portable Medical Devices," *Lecture Notes in Engineering and Computer Science*, vol. 2, Jun. 2010.

[7] L. Dong *et al.*, "Multifunctional pacemaker lead for cardiac energy harvesting and pressure sensing," *Advanced healthcare materials*, vol. 9, no. 11, p. 2000053, 2020.

[8] A. S. Manolis, T. Maounis, S. Koulouris, and V. Vassilikos, "'Real life' longevity of implantable cardioverter-defibrillator devices," *Clinical cardiology*, vol. 40, no. 9, pp. 759–764, 2017.

[9] S. P. Beeby *et al.*, "A micro electromagnetic generator for vibration energy harvesting," *Journal of Micromechanics and microengineering*, vol. 17, no. 7, p. 1257, 2007.

[10] B. Vysotskyi, D. Aubry, P. Gaucher, X. Le Roux, F. Parrain, and E. Lefeuvre, "Nonlinear electrostatic energy harvester using compensational springs in gravity field," *Journal of Micromechanics and Microengineering*, vol. 28, no. 7, p. 074004, 2018.

[11] Y. Lu *et al.*, "A batch-fabricated electret-biased wideband MEMS vibration energy harvester with frequency-up conversion behavior powering a UHF wireless sensor node," *Journal of Micromechanics and Microengineering*, vol. 26, no. 12, p. 124004, 2016.

[12] G. Bécan *et al.*, "Fabrication and mechanical study of a titanium micro-membrane for in vivo pressure monitoring," in *2020 14th International Symposium on Medical Information Communication Technology (ISMICT)*, 2020, pp. 1–6.

[13] S. D. Senturia, *Microsystem Design*. Springer US, 2001. doi: 10.1007/b117574.

[14] L. L. Howell, *Compliant Mechanisms*. John Wiley & Sons, 2001.

[15] G. K. Fedder, "Simulation of microelectromechanical systems," PhD Thesis, University of California, Berkeley, 1994.

[16] A. Karami, J. Juillard, E. Blokhina, P. Basset, and D. Galayko, "Electrostatic Near-Limits Kinetic Energy Harvesting from Arbitrary Input Vibrations," *arXiv preprint arXiv:2002.07086*, 2019.

[17] A. H. Hosseinloo and K. Turitsyn, "Fundamental limits to nonlinear energy harvesting," *Physical Review Applied*, vol. 4, no. 6, p. 064009, 2015.

[18] B. Vysotskyi, "Récupérateur d'énergie vibratoire MEMS électrostatique à large bande pour applications biomédicales," PhD Thesis, Université Paris-Saclay (ComUE), 2018.

[19] S. Roundy, P. K. Wright, and J. Rabaey, "A study of low level vibrations as a power source for wireless sensor nodes," *Computer communications*, vol. 26, no. 11, pp. 1131–1144, 2003.

[20] E. Lefeuvre, S. Risquez, J. Wei, M. Woytasik, and F. Parrain, "Self-biased inductor-less interface circuit for electret-free electrostatic energy harvesters," in *Journal of Physics: Conference Series*, 2014, vol. 557, no. 1, p. 012052.

[21] D. Galayko *et al.*, "Capacitive energy conversion with circuits implementing a rectangular charge-voltage cycle—part 1: Analysis of the electrical domain," *IEEE Transactions on Circuits and Systems I: Regular Papers*, vol. 62, no. 11, pp. 2652–2663, 2015.